Main Chain and Side Chain Dynamics of Peptides in Liquid Solution from ^{13}C NMR: Melittin as a Model Peptide†

Marvin D. Kemple,*,‡ Paul Buckley,§,|| Peng Yuan,‡,⊥ and Franklyn G. Prendergast§

Department of Physics, Indiana University Purdue University Indianapolis, Indianapolis, Indiana 46202-3273, and Department of Biochemistry and Molecular Biology and Department of Pharmacology, Mayo Foundation, Rochester, Minnesota 55905

Received August 26, 1996; Revised Manuscript Received December 2, 1996⊗

ABSTRACT: Peptide backbone and lysine and tryptophan side chain mobilities in the synthetic, 26-residue peptide melittin (MLT) enriched with ^{13}C were investigated in liquid solution by ^{13}C T_1 and steady state nuclear Overhauser effect measurements at two magnetic fields and by Trp fluorescence anisotropy measurements and were analyzed using the Lipari and Szabo model-free approach. The overall rotational correlation times at 20 °C were 1.28, 1.4, 2.8, and 4.2 ns for monomeric random coil MLT, for monomeric helical MLT (in CD_3OD), for tetrameric MLT in neat D_2O, and for the tetramer in 50 mM phosphate buffer, respectively. Motion of the backbone in the interior of the sequence was most restricted in the monomeric helix and least restricted in the tetramer. In the monomeric disordered peptide, relatively less restricted backbone motion extending from the N terminus to the fourth residue was observed. Such "end effects" continued only to the third residue in the monomeric helix and were observed just in the amino terminus glycine in the tetramer. The three Lys side chains showed the least restricted motion in the monomers and a differential restriction in the tetramers consistent with the tetramer structure. The motion of the Trp side chain was more restricted than that of Lys side chains and generally as restricted as that of the interior backbone atoms. The effective correlation times for the local motion of the backbone atoms were in the motional narrowing limit and showed distinct patterns. Agreement between NMR relaxation and Trp fluorescence anisotropy data was good for the monomer but not for the tetramer. Implications of these results for peptide dynamics in general are examined.

There has been substantial interest, especially during the last few years, in the dynamics of peptides (Blackledge et al., 1993; Chen et al., 1993; Dellwo & Wand, 1989; Hu et al., 1990; Palmer et al., 1991, 1993; Palmer & Case, 1992; Fan & Mayo, 1995; Friedrichs et al., 1995). This is not surprising in view of the role peptide dynamics must play, for example, in the function of peptide hormones as the latter approach and dock to their receptors or interact with membrane surfaces. Additionally, as proteins fold from a nascent polypeptide chain, peptide backbone and side chain dynamics inevitably influence to some extent both the kinetics of the process and the character of the final state achieved. However, despite the measure of current research interest and the number of studies ongoing, there are surprisingly few definitive data regarding the details (rates and amplitudes) of peptide dynamics or of the detailed kinetics of secondary and tertiary structure formation [cf. Hu et al. (1990), Palmer et al. (1991, 1993), Palmer and Case (1992), Fan and Mayo (1995), and Friedrichs et al. (1995)]. Nor do we have, for example, a consensus view of the transition rates between elements of secondary structure and random coils; for example, values for helix−coil transitions cited range between 10^{-8} and 10^{-5} s. Similarly, despite the current popularity of the molten globule concept [for a review, see Kuwajima (1989)], a key assumption of that hypothesis, namely increased mobility of the peptide backbone and side chains, has yet to be validated convincingly by direct measurement. How the dynamics of peptides contribute to all of these processes remains conjecture in part, we believe, because the requisite parameters describing peptide main chain and side chain mobility are hard to come by since there is as yet no single technique capable of yielding unequivocal quantitative results.

Our own approach has been to ask first whether the rates and amplitudes of motions of the peptide backbone and side chains can actually be reasonably quantified in relatively simple systems, and thereafter, we hope to probe the effects of such motions on the evolution of secondary and tertiary structure. To achieve these objectives, we have sought a model system capable of undergoing structural transitions from random form to a fully folded tertiary structure. The peptide melittin (MLT)[1] provides just such a model, and we believe that nuclear magnetic resonance relaxation measurements provide the most direct, quantitative data currently possible experimentally. MLT, a 26-residue peptide, which is a major component of the venom of the honey bee, *Apis mellifera*, is particularly useful for dynamical studies because (i) its conformation can be manipulated by varying the solvent conditions, (ii) under appropriate solvent conditions

† This work was supported in part by NSF Grant DMB-9105885 to M.D.K. and by PHS Grant GM34847 to F.G.P.

* Author to whom correspondence should be addressed.

‡ Indiana University Purdue University Indianapolis.

§ Mayo Foundation.

|| Present address: Department of Internal Medicine, St. Luke's-Roosevelt Hospital Center, 1111 Amsterdam Ave., New York, NY 10025.

⊥ Present address: Structural, Analytical, & Medicinal Chemistry, Pharmacia & Upjohn, Inc., Kalamazoo, MI 49001.

⊗ Abstract published in *Advance ACS Abstracts,* January 15, 1997.

[1] Abbreviations: CSA, chemical shift anisotropy; DSS, 2,2-dimethyl-2-silapentane 5-sulfonate, sodium salt; IUPUI, Indiana University Purdue University Indianapolis; MLT, melittin; NOE, steady state nuclear Overhauser effect; TMS, tetramethylsilane.

S0006-2960(96)02146-0 CCC: $14.00

it forms a tetramer which mimics a small globular protein, and (iii) it contains a tryptophan residue which allows direct comparisons of fluorescence anisotropy measurements of dynamics with those of NMR. [See Dempsey (1991) and Zhu et al. (1995b) for more details regarding the nature of MLT and references thereto.]

From ^{13}C relaxation rates (T_1 and NOE at two different magnetic fields), we have obtained values for the order parameter (which is a measure of the amplitude of the internal motion) and an effective correlation time for the internal motion for several backbone and side chain (Lys and Trp) positions in MLT synthesized with amino acids enriched in ^{13}C. The motional parameter values were obtained for MLT as a monomeric random coil in aqueous solution at pH 4, a monomeric helix in methanol, and a tetramer at pH 9 in aqueous solution both with and without phosphate. In addition in each case, a value for the correlation time for the overall rotational motion of the molecule was obtained. Furthermore, the NMR measurements were compared with steady state and time-resolved fluorescence anisotropy measurements on similar MLT samples. Generally, motion along the backbone was more restricted in the monomeric helix than in either the random coil or tetramer. Peptide "end effects" were apparent in the random coil but were reduced in the monomeric helix and tetramer. Finally, the agreement between the Trp fluorescence anisotropy and NMR relaxation results was good in some, but not all, cases.

MATERIALS AND METHODS

Materials. MLT, which has the sequence G*-I-G*-A*-V-L*-K†-V-L*-T-T-G*-L*-P-A*-L*-I-S-W†-I-K†-R-K†-R-Q-Q was enriched with ^{13}C at 14 different sites in five separately synthesized peptides as described previously (Yuan et al., 1996), where the specific backbone positions labeled (designated with an *) were [α-^{13}C]G1, [α-^{13}C]G3, [α-^{13}C]A4, [α-^{13}C]L6, [α-^{13}C]L9, [α-^{13}C]G12, [α-^{13}C]L13, [α-^{13}C]A15, and [α-^{13}C]L16 and the labeled side chain positions (designated with a †) were [ϵ-^{13}C]K7, [δ_1-^{13}C]W19, [ϵ_3-^{13}C]W19, [ϵ-^{13}C]K21, and [ϵ-^{13}C]K23. The enriched residues were limited to these based on their commercial availability and cost. Different labeling patterns were used in individual peptides to eliminate spectral overlap. The sample conditions were as follows: random coil monomeric MLT, 1 mM MLT in D_2O at pH 4 (uncorrected); monomeric helix, 1 mM MLT in CD_3OD; tetrameric MLT, 4 mM MLT in D_2O at pH 9, 2 mM at pH 10.5 (one sample), and 1 mM MLT in 50 mM phosphate buffer in D_2O at pH 9. The monomeric or tetrameric nature of MLT in the aqueous solutions was verified by reference to the work of Goto et al. (1992), by CD measurements, and directly by ^{13}C chemical shift measurements of the α-carbons (αCs). In particular, pH titrations of α-^{13}C chemical shifts of MLT [not shown, see Zhu et al. (1995b)] reveal at pH 4 a single peak for a given αC (with proton decoupling) which has a chemical shift consistent with a disordered structure (Wishart et al., 1991; Buckley et al., 1993). With increasing pH, the first peak does not shift but reduces in intensity and a second, 4−5 times broader, downfield-shifted peak, characteristic of a predominantly α-helical structure for MLT appears in slow exchange with respect to the original peak. At high pH (≥9), the precise value depending on the MLT concentration, only the α-helical peak, which we assign to the tetramer remains. Only one signal was observed from each labeled position in the tetramer, indicative of a nearly perfect symmetry for the conformation averaged on the chemical shift time scale. This behavior was observed in the presence or absence of 50 mM phosphate, the only difference being that the tetramer signal appears sooner with increasing pH in phosphate. The relaxation measurements presented here were performed on MLT near the end points of the titration. Note that the αC chemical shifts of MLT in methanol (see later) were very similar to those of the tetramer. This is expected since MLT is primarily helical and monomeric in methanol (Bazzo et al., 1988; Buckley et al., 1993).

NMR and Fluorescence Measurements. ^{13}C NMR measurements were conducted at the IUPUI NMR Center and at the Mayo Foundation by direct detection at 75.4 and 125.7 MHz on Varian Unity (Varian Associates, Palo Alto, CA) and Bruker AM (Rheinstetten, Germany) spectrometers. The 10 mm broad-band probes used with the Unity spectrometers were obtained from Cryomagnet Systems (Indianapolis, IN). Proton-decoupled ^{13}C spectra were obtained using broad-band noise decoupling during signal acquisition. In line with recent suggestions (Wishart et al., 1995), the ^{13}C spectra were referenced to DSS at 0 ppm using external dioxane at 69.28 ppm (measured specifically for our experimental conditions). Resonance assignments were made taking account of (i) the typical range of ^{13}C chemical shift values for each amino acid, (ii) the labeling scheme used in the individual peptides, (iii) published chemical shifts for MLT (Buckley et al., 1993; Yuan et al., 1996), and (iv) MLT pH titrations. The standard inversion recovery pulse sequence, $(\pi-t-\pi/2-\mathrm{Acq}-t_d)_n$, was used for T_1 measurements with more than 10 t values from 0.1 to 5 times the estimated T_1. The delay time, t_d, was at least $6T_1$. Proton decoupling during acquisition and saturation of the proton magnetization before inversion and during recovery of the ^{13}C magnetization were applied to eliminate effects from cross relaxation and from dipolar−CSA cross correlation (Boyd et al., 1990). The influence of dipolar cross correlation in cases where the carbon in question had two attached protons was minimized by deriving the T_1 values from fitting the recovery data out to approximately $3T_1$ to a three-parameter single-exponential magnetization equation (Zhu et al., 1995a). A similar procedure was followed for the carbons with a singly attached proton using data out to $5T_1$. Steady state $^{13}C-^{1}H$ NOE measurements were made by alternatively collecting ^{13}C signals with and without enhancement to account for instrument instability. The NOE values were obtained from ratios of the intensities or of the areas of the enhanced and equilibrium signals. The NMR measurements were made at a sample temperature of 20.0 ± 0.5 °C.

Steady state fluorescence intensity and anisotropy measurements were conducted at 20 °C with either a Perkin-Elmer MPF-66 (Norwalk, CT) or an SLM 8000 (Urbana, IL) fluorometer with excitation at 300 nm and detection at 345 nm for the monomer and 325 nm for the tetramer. Front-face techniques were used to avoid inner-filter effects so that the steady state fluorescence anisotropy measurements and the NMR measurements could be made at similar MLT concentrations. Time-resolved anisotropy and fluorescence lifetime measurements were made on samples at lower MLT concentrations (50 μM) at 20 ± 3 °C using a time-correlated photon-counting instrument with excitation at 300 nm and

detection at 340 nm. The tetramer in this case was formed in 50 and 150 mM phosphate at pH 9 in D_2O.

NMR Relaxation and Fluorescence Data Analysis. Although the equations used in the analysis have been given elsewhere [cf. Kemple et al. (1994)], they are repeated here for ease of reference within this paper. ^{13}C T_1 and NOE depend upon the magnetic dipolar interaction of the ^{13}C nucleus with its attached proton(s) and upon the CSA of the ^{13}C and are given by (Abragam, 1961)

$$T_1^{-1} = R_{DD}^{(1)} + R_{CSA}^{(1)} \quad (1)$$

$$NOE = 1 + {}^1/_4\, n\alpha^2 \frac{\gamma_H}{\gamma_C}\left[\frac{6J(\omega_H+\omega_C) - J(\omega_H-\omega_C)}{R_{DD}^{(1)} + R_{CSA}^{(1)}}\right] \quad (2)$$

where

$$R_{DD}^{(1)} = {}^1/_4 n\alpha^2[J(\omega_H-\omega_C) + 3J(\omega_C) + 6J(\omega_H+\omega_C)] \quad (3)$$

$$R_{CSA}^{(1)} = {}^1/_3\beta^2 J(\omega_C) \quad (4)$$

with

$$\alpha = \frac{\gamma_C\gamma_H\hbar}{r_{CH}^3} \quad \text{and} \quad \beta = {}^3/_2\omega_C\delta_{zz}\left(1 + \frac{\eta^2}{3}\right)^{1/2}$$

where ω_C and ω_H are the carbon and proton resonance frequencies, respectively, γ_C and γ_H are their respective gyromagnetic ratios, r_{CH} is the carbon−proton distance (fixed at 1.09 Å for our analysis), δ_{zz} is the largest magnitude principal element of the ^{13}C CSA tensor (in parts per million), n is the number of bonded protons, and η is the CSA tensor asymmetry parameter. [The relevant CSA parameters are given in Yuan et al. (1996).]

The spectral density, $J(\omega)$, given by Lipari and Szabo (1982) is used.

$$J(\omega) = {}^2/_5\left[\frac{S^2\tau_m}{1+\omega^2\tau_m^2} + \frac{(1-S^2)\tau}{1+\omega^2\tau^2}\right] \quad (5)$$

where S^2 is a generalized, motional model-free order parameter dependent on the amplitude of the internal motion of a given C−H vector ($0 \le S^2 \le 1$), and $\tau^{-1} = \tau_m^{-1} + \tau_e^{-1}$, where τ_e is an effective correlation time for the internal motion which has meaning when $S^2 < 1$ and $\tau_m \gg \tau_e$ is the correlation time for the overall rotational motion which is assumed to be isotropic. τ_m, S^2, and τ_e were extracted from least-squares fits of eqs 1−4 to the measured relaxation data using eq 5 with the computer program tau, a home-written C-language program which employs both Powell and Marquardt fitting algorithms, and with the program Modelfree 3.1, from A. G. Palmer. τ_m was obtained from global fits of data from all labeled residues for a given MLT conformer, and identical results (i.e. values within the calculated uncertainties) were obtained from the two analysis programs for all of the motional parameters. The overall quality of the fits was ascertained from $\chi^2 = (N - N_p)^{-1} \sum_{i=1}^{N}(m_i-c_i)^2/\sigma_i^2$, with N being the number of data points, N_p the number of parameters, m_i and c_i the measured and calculated experimental values, and σ_i, the estimated uncertainties in the measured values, and from fits of data sets generated from Monte Carlo simulations (500 in each case) as outlined by Mandel et al. (1995). The uncertainties in the parameters were obtained from the fits of the simulated data as given by Modelfree 3.1. In addition, the procedure of Mandel et al. (1995) was applied to aid in ascertaining the appropriate number of individual (local) motional parameters to use for a given labeled position. Apart from a limited number of instances for the tetramer (see below), the set $\{S^2, \tau_e\}$ was optimum.

Time-resolved fluorescence anisotropy decay data, $r(t)$, were fitted to the expression

$$r(t) = r_0[f_1 \exp(-t/\phi_1) + f_2 \exp(-t/\phi_2)] \quad (6)$$

with the program Globals Unlimited (Beechem & Gratton, 1988), where r_0 is the fundamental anisotropy, ϕ_1 and ϕ_2 are the rotational correlation times which satisfy $\phi_1 \gg \phi_2$, and f_1 and f_2 are their respective fractions with $f_1 + f_2 = 1$. Connection is made with the NMR motional parameters by recasting eq 6 as

$$r(t) = r_0 \exp(-t/\tau_m)[S^2 + (1 - S^2)\exp(-t/\tau_e)] \quad (7)$$

with $f_1 = S^2$, $\tau_m = \phi_1$, and $\tau_e = \phi_1\phi_2/(\phi_1 - \phi_2) \sim \phi_2$. It then follows from eq 7 that the steady state anisotropy, $\bar{r}$, can be written as

$$\bar{r} = r_0\left[\frac{S^2}{1+\tau_f/\tau_m} + \frac{1-S^2}{1+\tau_f(\tau_e^{-1}+\tau_m^{-1})}\right] \quad (8)$$

where τ_f is the mean fluorescence lifetime (Weaver et al., 1989). S^2 in eqs 7 and 8 can be expected to be the same as that in eq 5 only if the fluorescence emission (electric) dipole vector is parallel to the specific C−H vector. For Trp, there is uncertainty regarding the direction of the emission dipole, but it appears that it makes a smaller angle with the $C\delta_1$−H vector than it does with the $C\epsilon_3$−H vector (Lakowicz et al., 1983). Thus, S^2 from $C\delta_1$ in NMR should be compared with the fluorescence value. The steady state anisotropy was included along with the NMR data in the analysis for random coil MLT but not for the tetramer due to discrepancies in their predictions of the order parameters in the latter case (see later).

As groundwork to the presentation of the results, we need to discuss briefly the validity of the derived motional parameters. Questions unavoidably arise concerning the derivation of τ_m values from NMR relaxation data especially when transverse relaxation time (T_2, equations not given) data are used because T_2 is influenced by motions such as conformational exchange which occur on time scales considerably longer than τ_m and which are not accounted for in the spectral density (eq 5). For that reason, the approach taken in this work was extraction of motional parameters from T_1 and NOE data alone measured at two different magnetic fields. When T_2 values, which were measured in isolated cases (data not shown), were included, considerably larger τ_m values resulted. Recently, two groups (Jarvet et al., 1996; Lefêvre et al., 1996) have examined the interpretation of NMR relaxation rates using an approach introduced by Peng and Wagner (1992) in which values of the spectral density are derived at specific frequencies. Jarvet et al. (1996) concluded that S^2 values obtained in the Lipari and Szabo model-free approach appear to be robust but that τ_e is not. Lefêvre et al. (1996) found that reasonable results

Table 1: ^{13}C Chemical Shift and Relaxation Data for Random Coil Melittin in D_2O at pH 4[a]

		75 MHz		125 MHz	
residue	δ (ppm)[b]	T_1 (s)	NOE	T_1 (s)	NOE
G1α	42.97	0.28	2.13	0.39	2.07
G3α	44.84	0.16	2.24	0.22	2.15
A4α	52.29	0.25	1.98	0.39	1.82
L6α	54.88	0.19	1.87	0.30	1.77
L9α	54.90	0.19	1.83	0.30	1.72
G12α	44.90	0.13	1.67	0.20	1.57
L13α	53.37	0.20	1.76	0.29	1.61
A15α	52.45	0.20	1.69	0.32	1.61
L16α	55.70	0.19	1.59	0.32	1.45
W19δ_1	126.88	0.19	1.61	0.26	1.50
W19ϵ_3	120.77	0.17	1.44	0.25	1.41
K7ϵ	41.82	0.39	2.51	0.48	2.48
K21ϵ	41.81	0.41	2.56	0.49	2.49
K23ϵ	41.72	0.37	2.65	0.47	2.63

[a] Uncertainties in T_1 and NOE were ±5%. [b] Chemical shifts are referenced to DSS and were reproducible to ±0.05 ppm.

Table 2: ^{13}C Chemical Shift and Relaxation Data for Helical Melittin in 100% Methanol[a]

		75 MHz		125 MHz	
residue	δ (ppm)[b]	T_1 (s)	NOE	T_1 (s)	NOE
G1α	43.75	0.14	1.70	0.22	1.59
G3α	47.60	0.097	1.62	0.16	1.54
A4α	55.88	0.17	1.65	0.27	1.51
L9α	58.46	0.17	1.60	0.27	1.45
G12α	46.40	0.090	1.50	0.15	1.43
A15α	55.82	0.15	1.39	0.27	1.39
W19ϵ_3	120.97	0.16	1.58	0.20	1.44
K21ϵ	42.34	0.25	2.44	0.31	2.27

[a] Uncertainties in T_1 and NOE were ±5%. [b] Chemical shifts are referenced to DSS and were reproducible to ±0.05 ppm.

could be expected from the model-free analysis, keeping in mind that S^2 is related to the amplitude of motion on the subnanosecond time scale. Our experience is that, although the accuracy of the values of S^2 and τ_e may be questioned, the general concurrence of their values with expectation among atomic sites in a given MLT conformer and between corresponding sites in different MLT conformers supports their use in making physical inferences.

RESULTS

The measured ^{13}C chemical shifts are compiled in Tables 1−4 for the four MLT conformers studied: (i) random coil at pH 4 in D_2O, (ii) monomeric, primarily helical peptide in methanol, (iii) tetramer at high pH in D_2O, and (iv) tetramer at pH 9 in 50 mM phosphate. The relaxation data, which are also given in Tables 1−4, are averages of at least two measurements in the majority of cases. Uncertainties in the relaxation data were estimated on the basis of the repeated measurements. Trp steady state anisotropy measurements were made only on the random coil and on the tetramer in D_2O and were found to be 0.040 and 0.10, respectively. The average fluorescence lifetime in the two cases was 3.5 and 3.4 ns, respectively. An uncertainty of ±10% was used for these in the data-fitting procedures. The motional parameters obtained are summarized in Table 5 and described according to the assumed MLT conformation below.

Random Coil Melittin. The global τ_m value was 1.28 ± 0.09 ns. To verify the robustness of this value, the data also

Table 3: ^{13}C Relaxation Data for Tetrameric Melittin in D_2O at pH 9[a]

		75 MHz		125 MHz	
residue	δ (ppm)[b]	T_1 (s)	NOE	T_1 (s)	NOE
G1α	45.77	0.29	1.58	0.49	1.68
G3α	46.88	0.17	1.36	0.36	1.28
A4α	54.61	0.31	1.29	0.68	1.31
L6α	57.94	0.37	1.31	0.78	1.24
L9α	57.67	0.36	1.25	0.84	1.22
G12α	46.48	0.18	1.26	0.43	1.31
L13α	59.27	0.33	1.22	0.68	1.26
A15α	54.72	0.35	1.25	0.76	1.23
L16α	58.06	0.36		0.76	1.24
W19δ_1	126.95	0.28	1.29	0.50	1.20
W19ϵ_3	120.55	0.32	1.22	0.52	1.21
K7ϵ	41.75	0.36	2.49	0.45	2.22
K21ϵ	41.86	0.30	2.26	0.38	2.08
K23ϵ	41.85	0.27	2.17	0.36	2.00

[a] Uncertainties in T_1 and NOE were ±5%. The missing entry indicates that data were not available. [b] Chemical shifts are referenced to DSS and were reproducible to ±0.05 ppm.

Table 4: ^{13}C Relaxation Data for Tetrameric Melittin in 50 mM Phosphate Buffer at pH 9[a]

		75 MHz		125 MHz	
residue	δ (ppm)[b]	T_1 (s)	NOE	T_1 (s)	NOE
G1α	45.62	0.23	1.49	0.51	1.65
G3α	47.06		1.20	0.37	1.35
A4α	54.85	0.31	1.23	0.65	1.23
G12α	46.32	0.18	1.22	0.44	1.33
L13α	59.36			0.71	1.26
A15α	54.78	0.29	1.24	0.74	1.30
L16α	58.06	0.33	1.24	0.81	1.19
W19δ_1	127.78	0.30	1.20	0.49	1.35
W19ϵ_3	120.58	0.26	1.35	0.46	1.17
K7ϵ	41.75	0.34	2.43	0.48	2.46
K23ϵ	31.63	0.27	2.15	0.35	2.16

[a] Uncertainties in T_1 and NOE were ±5% apart from the Trp data, where the uncertainties were ±10%. Missing entries indicate that data were not available. [b] Chemical shifts are referenced to DSS and were reproducible to ±0.05 ppm.

were fitted allowing for individual τ_m values for each residue. Those values agreed with the global value within the errors in the parameters. Peptide end effects are evident in the order parameters given in Table 5 for the backbone atoms and illustrated in Figure 1. Specifically, S^2 values are in the order G1 < G3 < A4 < average of measured αC order parameters for L6−L16 (0.49). As will be seen to be the case for the tetramer as well, the order parameter for the αC of G12 is less than that for backbone positions other than the end residues. In terms of the side chains, the order parameters for the Cϵ position of the three lysines are all small ($\leq$0.05) and are identical within the experimental errors. If the motion of the Lys Cϵ−H vectors were axially symmetric about the Cδ−Cϵ bond, S^2, given by $^1/_4(1 - 3\cos^2\theta)^2$ with $\theta = 71°$ for tetrahedral geometry, would be $^1/_9$. That the observed S^2 values are $<^1/_9$ implies that additional motions are influencing the order parameter (e.g. motion of the Cδ−Cϵ bond itself) which is to be expected for a flexible aliphatic side chain such as Lys. The Trp side chain S^2 values are similar to the values obtained for the interior backbone positions.

τ_e values ranged from about 37 to 121 ps with no obvious pattern among the various residues. Similar values of τ_e were found for the backbone and the side chain positions, and all

Table 5: Motional Parameters for Monomeric, Helical, and Tetrameric Melittin from NMR[a]

	monomer		helix		tetramer		phosphate tetramer	
	$\tau_m = 1.28 \pm 0.09$ ns $\chi^2 = 0.98$		$\tau_m = 1.4 \pm 0.1$ ns $\chi^2 = 0.88$		$\tau_m = 2.8 \pm 0.2$ ns $\chi^2 = 2.2$		$\tau_m = 4.2 \pm 0.5$ ns $\chi^2 = 1.6$	
	S^2	τ_e (ps)	S^2	τ_e (ps)	S^2	τ_e (ps)	S^2	τ_e (ps)
G1α	0.13 ± 0.01	37 ± 4	0.36 ± 0.02	36 ± 7	0.19 ± 0.01	18 ± 2	0.29 ± 0.02	18 ± 3
G3α	0.19 ± 0.02	89 ± 10	0.54 ± 0.03	58 ± 15	0.37 ± 0.02	7 ± 3	0.48 ± 0.03	10 ± 4
A4α	0.35 ± 0.03	77 ± 11	0.63 ± 0.03	88 ± 25	0.40 ± 0.02	8 ± 4	0.53 ± 0.02	8 ± 4
L6α	0.46 ± 0.04	121 ± 21	–	–	0.34 ± 0.02	4 ± 3	–	–
L9α	0.48 ± 0.03	104 ± 19	0.65 ± 0.03	66 ± 24	0.34 ± 0.01	1 ± 2	–	–
G12α	0.40 ± 0.02	38 ± 9	0.62 ± 0.03	38 ± 17	0.33 ± 0.01	4 ± 3	0.42 ± 0.02	7 ± 3
L13α	0.52 ± 0.03	89 ± 18	–	–	0.39 ± 0.02	4 ± 3	0.52 ± 0.03	7 ± 7
A15α	0.51 ± 0.03	66 ± 15	0.74 ± 0.04	30 ± 17	0.37 ± 0.02	3 ± 2	0.51 ± 0.02	8 ± 4
L16α	0.58 ± 0.03	37 ± 15	–	–	0.36 ± 0.02	3 ± 3	0.47 ± 0.02	2 ± 2
W19ϵ_3	0.56 ± 0.03	35 ± 16	0.59 ± 0.04	100 ± 26	0.36 ± 0.02	6 ± 4	0.54 ± 0.05	14 ± 11
W19δ_1	0.53 ± 0.03	63 ± 17	–	–	0.44 ± 0.02	7 ± 4	0.52 ± 0.04	21 ± 10
K7ϵ	0.05 ± 0.01	41 ± 4	–	–	0.07 ± 0.01	43 ± 3	0.09 ± 0.01	45 ± 3
K21ϵ	0.05 ± 0.01	41 ± 3	0.10 ± 0.01	62 ± 5	0.13 ± 0.01	47 ± 4	–	–
K23ϵ	0.04 ± 0.01	46 ± 3	–	–	0.14 ± 0.01	46 ± 4	0.16 ± 0.02	54 ± 4

[a] Residues for which data were not available are indicated by dashes. The errors listed in the parameters were derived from Monte Carlo simulations based on the uncertainties in the measured quantities. The number of degrees of freedom used in the χ^2 calculations was 29, 15, 27, and 20 for the monomer, helix, tetramer, and phosphate tetramer, respectively.

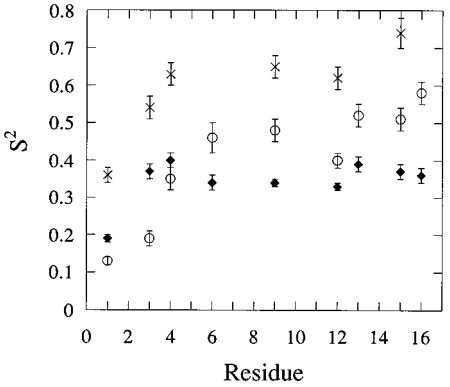

FIGURE 1: Cα order parameters for melittin by sequence number from Table 5. ○ represents the random coil monomer, × the helical monomer, and ◆ the tetramer. The error bars are based on the uncertainties listed in Table 5.

were in the NMR motional narrowing limit ($\omega\tau_e < 1$ at the relevant frequencies). τ_e values of similar magnitude were found in a Zn-finger peptide (Palmer et al., 1991).

MLT Helix in Methanol. As was the case for the random coil monomer, τ_m for the monomeric helix in methanol was well-defined with the value 1.4 ± 0.1 ns. Inspection of the results in Table 5 and Figure 1 reveals some significant differences between the MLT monomeric helix and the random coil monomer, the most obvious being the consistently larger order parameters found in corresponding positions of the monomeric helix. This is certainly a reasonable result for the backbone given the inherently greater order given to the helical form by the hydrogen-bonding network. End effects are also clearly less pronounced in the helix. G1 and G3 still have smaller order parameters than other backbone sites, but the putative end effect does not extend as far as A4. Interestingly, the τ_e values of the helix are similar to those of the random coil, the only pronounced differences being the occurrence of larger values of τ_e for Lys-21 and W19ϵ_3 in the helix.

The approximate cylindrical symmetry of the monomeric MLT helix makes anisotropic motion inevitable. The extent to which such anisotropic motion influences the recovered motional parameters must be considered. This can be assessed by still expressing the motional autocorrelation function as a product of terms representing the overall and the internal motions, but with the former modified to include three terms [cf. Barbato et al. (1992) and Mackay et al. (1996)]. Each term contains a rotational correlation time and is weighted by a factor which depends on the angle of a particular C−H vector and the symmetry axis of the molecule. There is a numerical relationship among the three correlation times, so if the geometric factors are known, this amounts to adding one additional parameter. For a relatively flexible peptide such as melittin, it is by no means certain that these factors are well-defined. We nonetheless estimated the effects of a modified correlation function on our results as follows. First, although MLT forms a bent helix in methanol (Bazzo et al., 1988), we approximated it as a prolate ellipsoid with an axial ratio of 3:1 from the coordinates of the MLT helix obtained from the structure of MLT in MLT/micelle complexes (Ikura et al., 1991). (The coordinates for MLT in methanol are not available.) Second, the effective overall correlation time (Barbato et al., 1992) was put equal to τ_m (Table 5). Third, the calculations given by Small et al. (1991) were used to derive specific numerical values for the three overall correlation times, and fourth, the geometric factors were evaluated using the coordinates noted above. We found that the *maximum* spread of calculated T_1^{-1} values across the labeled positions averaged 5.6% at 7*T* and 11*T* and that the maximum difference between the isotropic and anisotropic spectral densities at any one position averaged 6.6%. There is thus no advantage to using a more complex and additionally parameterized spectral density in the analysis of these data.

MLT Tetramer. For this conformer, τ_m was found to be 2.8 ± 0.2 ns. Intuitively, one would expect τ_m to be larger for the tetramer than for the monomers, as was observed, how much larger being dependent on the structures and their associated rotational friction. Effects from anisotropic overall motion should be even smaller for the tetramer than for the monomeric helix since the tetramer more closely approximates a spherical shape, and thus, they were neglected.

Some interesting initial observations can be made from the motional parameters in Table 5. First, the end effect is now apparent for G1 only (see Figure 1). Second, the order

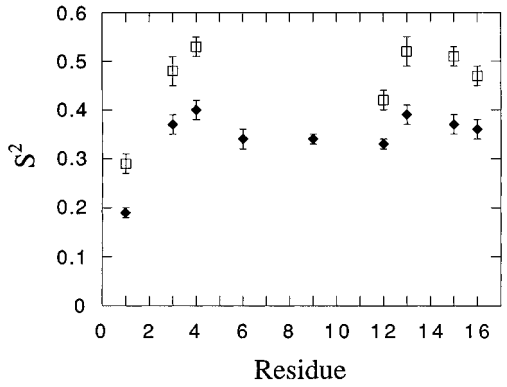

FIGURE 2: Comparison of Cα order parameters for melittin by sequence number from Table 5 for the tetramer (◆) and the phosphate tetramer (□). The error bars are based on the uncertainties listed in Table 5.

parameter for G12 is less than the average value of S^2 of the other backbone order parameters (0.37), excluding G1. Third, the Trp side chain order parameters were comparable to the backbone order parameters. And fourth, the Lys order parameters fell in the sequence K7 < K21 ≤ K23. Except for G1 and G3, the backbone order parameters are smaller individually in the tetramer than in the random coil monomer. For the side chains, the tetramer order parameters are smaller for Trp, larger for K21 and K23, and of comparable value for K7 as compared with those of the random coil. A notable difference between the random coil and the tetramer was that the latter consistently gave smaller τ_e values except for the Lys side chains.

Since τ_e is small for several of the residues, it might be expected that the data could be fit well enough using S^2 only. However, using the *F* statistic, we found that inclusion of τ_e was statistically significant for the majority of the labeled positions. Accordingly, for purposes of consistency and comparison, τ_e values were given in Table 5 for each position. We also found that, while inclusion of an additional order parameter (Clore et al., 1990) for the Lys-21 and Lys-23 side chains reduced noticeably the differences between their measured and calculated relaxation data, the improvement was not statistically significant.

MLT Tetramer in Phosphate Buffer. The best fit of the relaxation data for the tetramer in 50 mM phosphate yielded a τ_m of 4.2 ± 0.5 ns which is larger than τ_m found for the tetramer formed in D_2O alone. Although fewer positions were examined for the phosphate tetramer, the trends in the S^2 and τ_e values were similar to those observed in the tetramer in D_2O as is evident in Figure 2. The tetramer in phosphate did manifest larger S^2 values, however, than did the tetramer in D_2O, whereas the τ_e values were generally similar for the two. The comments made in the preceding paragraph concerning the appropriate number of local parameters for the tetramer also apply here.

DISCUSSION

This discussion covers items specific to MLT and to peptide dynamics in general. Since the order parameter has been consistently the most commonly considered indicator of mobility, we begin with a consideration of how S^2 behaves in the structures we have studied. First, the backbone C−H vectors for the N terminus residues through A4 of the random coil show increased mobility relative to that of C−H vectors of residues more centrally located in the sequence. Introduction of secondary structure (α-helix) reduces the extent of these end effects in that G1 and G3, but now not A4, show an increased mobility relative to other backbone residues in the monomeric helix. In the MLT tetramer, only G1 retains a substantially increased mobility showing the restraining effect of tertiary interactions on peptide backbone motion. Interestingly, although G12 is near the center of the MLT sequence, it had a smaller order parameter than did the other backbone positions beyond A4 in the random coil and the tetramer, presumably reflecting the inherent flexibility of Gly residues.

The extent to which end effects penetrate the peptide chain has not apparently been investigated systematically with peptides of different lengths. Friedrichs et al. (1995) reported such effects for only the amino and carboxy terminal residues in a nine-residue, β-hairpin-forming peptide, but their S^2 values were generally larger than those observed here. Palmer et al. reported end effects in two residues at the carboxy terminus of a 25-residue Zn-finger peptide, whereas Frank et al. (1995) reported effects four residues in for the urea-denatured state of a small protein. Fan and Mayo (1995), who studied a 27-residue peptide in trifluoroethanol, saw only small effects on S^2 for either terminal residue, probably in keeping with the helical form of their peptide. In an interesting application of fluorescence anisotropy measurements, using an optimized Rouse−Zimm model, Hu et al. (1990) theoretically predicted slightly more extensive end effects in a 17-residue peptide than we found. Their experiments involved putting Trp residues at three different locations along the peptide chain and interpreting their fluorescence anisotropy decay data in terms of an average correlation time. They detected some apparent end effects, but the coincidence of theory with the experimentally derived motional parameters was not good. The failure may reside in the relative insensitivity of Trp side chain motion to peptide backbone mobility, an issue likely to affect any side chain-based assessment of main chain motion [cf. Miick et al. (1993) and Mchaourab et al. (1996)]. Note that end effects have been observed also in proteins [cf. Buck et al. (1995)].

Somewhat surprisingly, the monomeric helix in methanol had the most restricted internal motions. Consistently larger values for backbone order parameters were obtained relative to those seen in the random coil and the tetramer in neat D_2O, apart from the end effects just noted. If there are similar patterns of motion of the backbone C−H vectors in the different conformations, then larger S^2 values for the monomeric helix would indicate that the C−H vectors sample a smaller region of space in the monomeric helix than in the random coil peptide or the tetrameric structure. There is no easy way to rationalize this result intuitively, particularly in view of the fact that S^2 increases in the order tetramer < random coil < monomeric helix for the interior residues. For example, the stabilizing effect of the hydrogen-bonding network in the monomeric helical form provides, in principle, a reasonable explanation for a change in end effects and for the increased rigidity of that form relative to the random coil. But the peptide is also fully helical in the tetramer, and additionally, peptide motion should be stabilized further by the tertiary (interhelical) interactions in the oligomer, all of which points intuitively to the likelihood of higher, not lower, order parameters in the tetramer than in

either of the monomeric species. In pH titrations of the monomer and tetramer, we have observed exchange between them that is slow on the chemical shift time scale. Although subnanosecond dynamics do not relate directly to this exchange process, the smaller than expected order parameters in the tetramer do indicate a potential flexibility of the tetramer that ultimately would enhance the monomer−tetramer interconversion. The readiness of the tetramer to interchange with the monomer may imply that the tetramer structure is rather loose.

The values of τ_e clearly are smaller at backbone positions and for the Trp side chain in the tetramer formed at high pH in D_2O and the tetramer in phosphate relative to those of the monomers (see Table 5). As outlined by Lipari and Szabo (1982), if the correlation function of the internal motion represents Markovian processes and is expressed as a sum of exponential terms, $\sum_{i=1}^{n} a_i \exp(-t/\tau_i)$, where the sum is over n internal correlation times, $\tau_i \ll \tau_m$ weighted by the coefficients a_i, then τ_e is just the average of the internal correlation times, $\sum_{i=1}^{n} a_i\tau_i / \sum_{i=1}^{n} a_i$. Thus, a larger value for τ_e such as those found for the backbone in the monomers does not imply that faster motions are necessarily absent in the monomer but rather the reverse, namely that slower motions are absent or of less importance in the tetramer where τ_e was small. The lack of significant internal motion on a longer time scale for the backbone in the tetramer in turn implies that there is reduced internal friction in the tetramer relative to the monomer which is consistent with the expected more tightly packed structure of the tetramer and a reduced solvent exposure. A similar reasoning applies to the Trp residue as well. Small τ_e values have also been seen for backbone positions in a complex of a peptide with a protein (Chen et al., 1993). Interestingly, for a given MLT sample, including the tetramers, the Lys side chains as well as the amino terminal Gly residue gave distinctly larger values for τ_e. This is plausibly attributable to the net effects of counterions (especially in the phosphate) and electrostricted water, both of which would effectively add bulk to the cationic side chains and to the effects of viscous drag imposed by the solvent.

At this juncture, some comments on recovered τ_m values should be made. For a peptide that has little or no defined secondary structure, i.e. it is in all intents and purposes a random coil, then while its translational hydrodynamic behavior may be described in terms of a radius of gyration, there is really no analogous parameter for describing its rotational diffusion or rotational correlation time. However, the use of τ_m, S^2, and τ_e to describe the relaxation data was quite robust here for the random coil monomer. On the other hand, in disordered proteins, such has seemingly not been the case (Alexandrescu & Shortle, 1994). From our experience, and information available in the literature, it appears that an unstructured peptide will generally manifest a τ_m of ~1 ns with essentially equal S^2 values along the backbone far enough from the ends of the peptide, provided the peptide is sufficiently large (mass ≥ 2.5 kDa). In disordered proteins, the situation is more complex, with the system apparently behaving like a collection of peptide segments. From the results reported in this paper, it is clear that random coil melittin is not acting as a molecule composed of uncoupled segments since end effects were apparent and none of the backbone S^2 values was near zero. In any event, there is no simple way to compare τ_m for a random coil to τ_m for the monomeric helix, the latter having roughly cylindrical symmetry, to τ_m for the compact, largely ellipsoidal tetramer. The roughly 2−3-fold increase in τ_m as one goes from monomer to tetramer thus may be mostly fortuitous and essentially unrelated to the 4-fold increase in molecular mass. In the NMR method, one is measuring the apparent motion of individual vectors; i.e. one is determining the motion essentially of a single atom along the peptide chain or in an aromatic ring in the case of Trp. In the latter instance, because of the orientation of the C−H vectors relative to the essentially planar, effectively rigid ring, the motion of either the $C\delta_1$−H or $C\epsilon_3$−H vectors reasonably reflects motion of the entire ring. An analogous situation obviously cannot hold for atoms in the peptide chain. Nevertheless, current theory and our somewhat limited data lead us to use the Lipari and Szabo formalism (Lipari & Szabo, 1982) to analyze the relaxation data of the peptide backbone.

This said, it is interesting that τ_m is larger for the phosphate tetramer (4.2 ± 0.5 ns) than for the tetramer formed at high pH and concentration in D_2O (2.8 ± 0.2 ns). The difference in these numbers is consistent with the presence of phosphate groups "bound" to MLT. In particular, at pH 9, each MLT monomer composing the tetramer should have a charge of +5 (Zhu et al., 1995b). Thus, on the order of 10 phosphate ions per tetramer would be required to neutralize the charge at that pH [cf. Podo et al. (1982), who inferred the existence of five or six bound phosphate ions per monomeric unit of MLT at pH 7]. The presence of 10 phosphate ions would add an additional mass of ~1 kDa which would increase the rotational correlation time of the phosphate tetramer by an estimated 0.4 ns, calculated from the Stokes−Einstein relationship strictly on the basis of mass increase without the addition of hydration water. This increase is consistent with our results. There were also other signs of differences between the two tetrameric forms, namely that the backbone order parameters were consistently larger in the phosphate tetramer (Figure 2) and roughly the same size as the order parameters observed in the random coil monomer. Apparently, the tetramer formed in phosphate has a more rigid structure than that formed in the absence of phosphate.

Molecular Models. Although it is not possible to construct a single-parameter model that directly reflects the motion of the peptide backbone, it is still possible to obtain a notion of the amplitude of the motion by using a simple model. In particular, we will make use of the restricted diffusion model (London & Avitabile, 1978; Weaver et al., 1989) in which the motion is constrained to an angular range of $\pm\xi$ about the Cα−C′ bond (the traditional angle ψ) or the N−Cα bond (the traditional angle ϕ) to estimate the range of motion consistent with the order parameter values for a tetrahedral geometry. In this case, $S^2 = {}^1/_9 + 0.297\,[(\sin\xi)/\xi]^2 + 0.592\,[(\sin 2\xi)/2\xi]^2$, and we find that for $\xi = 45$, 50, and 60° the corresponding S^2 values are 0.59, 0.53, and 0.42 which are in the range of order parameters found in the interior of the sequence of random coil MLT. G1, G3, and A4 give a somewhat larger range of motion, their respective ξ values being 155, 115, and 65°, respectively, giving an idea of the magnitude of the end effects which in keeping with intuition decrease as one moves away from the amino terminal residue. While a jump model for G1, which would have to consist of three or more jumps since S^2 is near ${}^1/_9$, may be

appropriate, it gives no additional insight into the nature of these end effects.

Our results for the monomeric helix can be compared directly with molecular dynamics simulations of a polyalanine helical peptide (Daggett et al., 1991) which gave mean square fluctuations of both the ϕ and ψ dihedral angles of 11−13°. For A15 and G12, $S^2 = 0.74$ and 0.62, respectively, which represent the range of order parameter values for the interior backbone residues and correspond to $\xi = 34$ and 43°, respectively. The smaller S^2 for G1 yields a ξ of 66° to be compared with dihedral angle fluctuations of 23−34° in the simulation for terminal residues. Considering that the restricted diffusion model only accounts for motion in one angular variable, the roughly doubled experimental numbers are in good agreement with the numbers from the simulation.

Similar calculations can be done for the tetramer. As an illustration, the mean order parameter for the tetramer in Table 5 for G3−L16 (0.36) gives a ξ of 66°, while the corresponding mean order parameter for the phosphate tetramer in Table 5 (0.49) gives a ξ of 53°. Clearly, from our data, or for that manner any data extant in the literature, one cannot prove a particular model of the motion. The values we calculate here are, however, fundamentally compatible with the so-called "crankshaft model" of peptide bond motion (Daggett et al., 1991). Other mathematical models applied to the data will yield different numbers, but the pattern of implied mobility along the melittin backbone must be consistent.

In a like manner, differences in the order parameter values of the Cϵ−H vectors of the Lys residues from one form of MLT to the next can be rationalized. In the monomer, S^2 was the same for K7, K21, and K23 as would be expected in the disordered environment, and the values were substantially smaller than those of K21 and K23 in the helix and tetramer. For the tetramer, S^2(K7) < S^2(K21) ∼ S^2(K23). Inspection of the structure of the MLT tetramer obtained from X-ray crystallography (Terwilliger & Eisenberg, 1982a,b) shows clearly that the K7 side chains have few packing constraints on their motion; each of the four in the tetramer protrudes into the solvent. On the other hand, the K21 and K23 side chains are more sequestered. Thus, it is appropriate that the smallest value of S^2 is associated with K7 in the tetramer. The larger value of S^2 for K21 in the monomeric helix relative to its value in the random coil is in keeping with the more generally ordered environment in the helix.

As was the case for the backbone, it is difficult to construct a physically precise model that is entirely suitable for the Lys side chains since the Cϵ−H vector is at the penultimate position in the side chain and the Lys side chain has several degrees of freedom; nonetheless, a useful visualization can be achieved. If the motion of the Cϵ−H vector is axially symmetric about the Cδ−Cϵ bond, then for tetrahedral geometry, the measured order parameter can be written as $S^2 = {}^1/_9 S_{AXIS}{}^2$, where $S_{AXIS}{}^2$ is the order parameter describing the motion of the Cδ−Cϵ bond. This sort of motion implies $S^2 < {}^1/_9$ which holds for K7, K21, and K23 in the monomer and for K7 in the tetramer. First, just considering those cases, we find $S_{AXIS}{}^2$ to be 0.45 for the monomer (using an average order parameter of 0.05 for the three Lys residues) and 0.63 for K7 in the tetramer. It then follows that, if the Cδ−Cϵ bond (axis) is constrained to move within a cone of half-angle α (Kinosita model, Kinosita et al., 1977), $S_{AXIS}{}^2 = {}^1/_4 \cos^2\alpha(1 + \cos\alpha)^2$, where $\alpha = 40$ and 31° for the monomer and tetramer (K7), respectively. The more restricted motion of K21 and K23 in the tetramer is undoubtedly a combination of restriction of motion about the Cδ−Cϵ bond and of the Cδ−Cϵ bond itself. To obtain an estimate of the motion, we will assume that the main restriction is about the Cδ−Cϵ bond and make the approximation that $S^2 \approx S_{AXIS}{}^2 S_{AA}{}^2$, where $S_{AA}{}^2$ is the order parameter describing motion about the Cδ−Cϵ bond. Using the value of $S_{AXIS}{}^2$ found for K7 in the tetramer along with a restricted diffusion model for the motion about the axis as we did above for the peptide backbone, we calculate the angular extent of motion about the axis to be on the order of ±100°.

Motional models can also be developed for the Trp side chain whose motion we found to be considerably more hindered than that of the Lys side chains as reflected in the higher S^2 values for Trp. In this work, S^2 of W19 in the random coil was larger than that in the tetramer and of comparable value to that in the monomeric helix (Table 5). A distinction among the samples concerns the relative values of the order parameters for the Trp Cδ_1 and Cϵ_3 positions. For the tetramer in D_2O, S^2(Cδ_1) > S^2(Cϵ_3) which is similar to what we found for MLT in a micellar environment (Yuan et al., 1996), but for the random coil monomer and the phosphate tetramer, S^2(Cδ_1) ≈ S^2(Cϵ_3). This could imply a change in the nature of the Trp side chain motion in the different circumstances or may simply indicate increased freedom of motion of the indole moieties in the tetramer formed without the use of phosphate.

The simplest models for Trp involve motion only about the β−γ bond. However, a restricted diffusion model in which the indole ring rotates about the β−γ bond in an angular range of ±ξ gives inconsistent results for the monomer and tetramer. Specifically, since the Cδ_1−H and Cϵ_3−H vectors make different angles with respect to the β−γ bond, namely ∼72 and 26°, respectively, in tetrameric MLT with similar values presumably holding for the monomeric species, their order parameters are quite different for the same value of ξ. Or, conversely, similar order parameter values imply much different values of ξ. For example, using the values of S^2 for the random coil monomer in Table 5, we find that $\xi \sim 49$ and 130° from S^2 for Cδ_1−H and Cϵ_3−H, respectively; clearly, these are not compatible. Motion about the α−β bond could reduce the Cϵ_3−H order parameter relative to that of the Cδ_1−H vector depending on the angle the vectors make with respect to the α−β bond and could reduce the above discrepancy. Interestingly, a model in which the indole ring jumps about the β−γ bond between two equally populated sites separated by ∼145° is consistent with the results for the random coil monomer, but models involving 180° jumps are not. On the other hand, a two-site jump model is not compatible with the data for the tetramers no matter what the jump angle.

If, instead, motion about the β−γ bond is ignored and motion about only the α−β bond is considered, a three-site jump model in which the Trp moiety makes jumps of 120° about the α−β bond, where $S^2 = {}^1/_4(3\cos^2\theta_0 - 1)^2 + {}^3/_4(\sin^4\theta_0 + \sin^2 2\theta_0)(p_1{}^2 + p_2{}^2 + p_3{}^2 - p_1p_2 - p_2p_3 - p_1p_3)$, [$p_1$, p_2, and p_3 are the relative populations of the three sites ($p_1 + p_2 + p_3 = 1$), and θ_0 is the angle the vector makes with the α−β bond], gives relatively consistent results for the tetramer where we have values for θ_0 available from the X-ray crystal structure (Terwilliger & Eisenberg, 1982a,b)

of 85.4 and 62.4° for $C\delta_1-H$ and $C\epsilon_3-H$, respectively. Relative populations of the three sites of 0.7, 0.2, and 0.1 give $S^2(\delta_1) = 0.48$ and $S^2(\epsilon_3) = 0.33$ to be compared with the experimental values for the tetramer in Table 5. Clearly, the actual motion of the Trp ring must involve rotations about both the $\alpha-\beta$ and $\beta-\gamma$ bonds. The order parameter does not factor, however, because the motion about $\beta-\gamma$ is not axially symmetric on the basis of the order parameter values. Thus, we are constrained to examining either/or situations. These results stress the importance of devising independent notions of what the motion could be from other avenues such as molecular dynamics simulations, fluorescence lifetime measurements, or measurement of scalar coupling constants. Order parameters from relaxation measurements could be used subsequently to test the hypotheses.

Difficulties in choosing an appropriate model notwithstanding, we can use the Kinosita model (Kinosita et al., 1977) simply to give a physical "feel" for the range of motions available to the Trp ring. In particular, from the order parameters in Table 5 for the random coil monomer, the helical monomer, the tetramer in D_2O, and the phosphate tetramer, respectively, we find cone half-angles of 36, 33, 43, and 36° which do not differ greatly from one another, where in each conformer, where appropriate, the angles obtained from the $C\delta_1$ and $C\epsilon_3$ order parameters are averaged.

Comparison with MLT/Micelle Complexes. Given the apparent similar helicities of MLT in its complexes with detergents and in lipid monolayers (Ikura et al., 1991), a comparison of the dynamics of the soluble and micelle-bound MLT (Yuan et al., 1996) is useful. We stress six specific points. First, no end effects in MLT were apparent in the micelle complexes; thus, even S^2 for the G1 $C\alpha-H$ vector was comparable to the values at other backbone sites. A similar observation was made for a small peptide when bound to calmodulin (Chen et al., 1993). Second, the backbone order parameter values in the micelle complexes were distinctly larger than those of the MLT random coil monomer and the tetramer but very interestingly were generally comparable to S^2 of the MLT monomeric helix. Given the much larger molecular mass of the MLT/micelle complexes, this latter similarity of S^2 values is either a consequence of anomalies in the analysis of the spectral densities or, more likely, reflective of an intrinsic property of the stably helical peptide. Again, the contrasting results for backbone S^2 values in the tetramer need to be recalled. MLT tetramer does not denature but exchanges with the monomer as noted above; i.e. there is a ("random coil") monomer to tetramer equilibrium with no detectable evidence of intermediate dimer or monomeric helical forms (S. Venyaminov and F. G. Prendergast, unpublished data). *A priori*, we expect that exchange between free and micelle-bound MLT is likely to be slower; perhaps this is reflected in the S^2 values. Third, in the lipid complexes, order parameter values of the backbone positions in the latter part of MLT (G12, L13, A15, and L16) were smaller than those in the front. Such a pattern was not observed in any of the forms of MLT examined here. Fourth, the mobilities of the Lys side chains were more restricted in the micelle complexes than in the MLT monomers and the tetramers, although the same order of relative mobility prevailed [S^2(K23) > S^2(K21) > S^2(K7)] in the tetramer and the MLT/lipid mixed micelle. Fifth, the Trp side chain order parameters generally were larger in the lipid complexes.

Table 6: Summary of Motional Parameters for Trp-19 in Melittin from Time-Resolved Fluorescence Anisotropy Measurements[a]

sample	r_0	τ_m (ns)	S^2	τ_e (ps)
random coil monomer	0.31 (fixed)	1.2	0.65	71
	0.25	1.0	0.69	160
helical monomer in methanol	0.31 (fixed)	1.2	0.66	40
	0.25	1.4	0.75	214
tetramer in phosphate	0.31 (fixed)	2.2	0.55	38
	0.23	2.5	0.66	232

[a] Values presented are averages from three (random coil monomer) and two (helical monomer and tetramer) different samples. Standard errors in the fitted parameters are ±10%.

Apparently, the Trp ring is more strongly anchored in the micelle complex. Sixth, the values of τ_e in the micelle are on the same order as those in the random coil and helical monomers but larger than the corresponding values found for the tetramer. Although overall the internal motion of MLT is more restricted in the micellar complexes, the similarity of the $C\alpha$ order parameters in the micelles and the helical monomer could be indicative of similar hydrogen-bonding networks in the two cases.

NMR Relaxation and Fluorescence Anisotropy Comparisons. The results of Trp time-resolved anisotropy measurements are summarized in Table 6. The anisotropy decay data were fit to eq 6, and the parameters given in Table 6 are calculated from eq 7. The initial anisotropy (r_0) was either fixed at 0.31 (Valeur & Weber, 1977) or allowed to vary, the latter circumstance yielding only slightly better fits (a reduction in χ^2 of 0.1 or less). As mentioned previously, we expected the fluorescence order parameter to correspond more closely to the NMR order parameter for the Trp $C\delta_1-H$ vector since the fluorescence emission vector is closer in orientation to that vector than it is to the $C\epsilon_3-H$ vector. For the MLT random coil and helical monomers, there is good agreement of the motional parameters from NMR (Table 5) and fluorescence (Table 6), especially for the apparent τ_m. However, for tetrameric MLT (in phosphate), the fluorescence-derived τ_m values were consistently smaller than the NMR values. A similar discrepancy in τ_m values was reported for a partially structured Zn-finger peptide (Palmer et al., 1993).

Trp steady state anisotropy data measured on samples at "NMR concentrations" were included in the fitting of the NMR data for the random coil monomer, but it is also possible to use eq 8 to estimate the order parameter from the steady state anisotropy data alone given τ_m, τ_e, and the fluorescence lifetime (τ_f). As long as $\tau_e \ll \tau_m$, this procedure yields a value for S^2 that is only weakly dependent on τ_e. Values of S^2 calculated using $r_0 = 0.31$ and $\tau_f = 3.5$ ns were 0.45 and 0.72 with uncertainties on the order of ±15% for the random coil monomer and the tetramer formed in neat D_2O. The agreement with the results from Table 5 is good in the former case and poor in the latter.

Overall, both the time-resolved and steady state Trp fluorescence anisotropy results agree reasonably well with the NMR relaxation results for the random coil monomer, and time-resolved fluorescence anisotropy is consistent with NMR for the helical monomer. For the tetramer, the results from the two techniques do not agree, especially with regard to τ_m and the tendency for the fluorescence data to give higher S^2 values. Why do these differences exist? One possibility is the MLT concentration. The steady state anisotropy and the NMR experiments were carried out at

similar MLT concentrations, but the time-resolved anisotropy data were taken at considerably lower concentrations. The nature of the tetramer itself is solvent- and concentration-dependent which could be reflected in the dynamics. Differences in order parameters between the two techniques may relate to misorientation of the fluorescence emission vector and the $C\delta_1-H$ vector. Other potential problems relate to the degree of anisotropic motion of the tetramer which could affect the parameters unevenly in the two techniques. The question of whether the fluorescence and NMR measurements of dynamics are quantitatively consistent is thus still not answered from these experiments. On the other hand, there is a qualitative conformity in the results derived from the two approaches.

SUMMARY

Although all of our work has focused on MLT, we believe that a number of the results will be applicable substantially to (unstructured) peptides. General and specific aspects of the work are summarized below.

(1) In peptides devoid of secondary structural elements, the peptide backbone will show higher mobility for residues in as far as the third or fourth amino acid. Beyond that, the apparent mobilities at any internal site will probably be about equal (i.e. have approximately the same S^2 and τ_e) except for glycine residues which will invariably be more flexible.

(2) We believe that an *apparent* τ_m of approximately 1 ns will be the typical value found for randomly structured peptides, although we cannot predict the peptide length dependence of this value. This τ_m most likely reflects not the motion of the peptide as a whole but the value recovered for a randomly flexing peptide chain.

(3) Adoption of secondary structure (in our case α-helix) in the monomeric peptide with no increase in molecular mass led to distinctly higher order parameters. Similar observations have been made in other systems [e.g. see Farrow et al. (1995) and Buck et al. (1995)]. In such a case, the recovered τ_m is probably related to the particular geometry of the peptide induced by the secondary structure.

(4) Although intuitively one might expect the motions of an aromatic side chain such as that of Trp to show largely unrestricted motion, it seems that the relatively apolar character of the indole moiety promotes interactions either with adjacent side chains or with the main chain which reduce mobility as is evident in the S^2 values we have described.

(5) In contrast, mobilities of charged side chains such as lysines are nearly unrestricted as expected.

(6) We have no consistent evidence that side chain motion *in peptides* readily reflects local backbone mobility (cf. Trp in the random coil monomer and the helical monomer). This conclusion raises concerns regarding attempts to define or quantify peptide backbone motion from measurements (fluorescence, EPR, or NMR) done on peptide side chains per se or on chemically labeled peptide side chains.

(7) Despite the obvious inherent limitations of the Lipari and Szabo model for calculating mobility parameters for intrinsically anisotropic motions such as those of a flexible peptide, the parameters recovered are internally consistent and the values (for S^2 and τ_e) seem physically reasonable. Here, when MLT assumed tertiary structure in the tetramer, the results from the analysis are, interestingly, not necessarily less problematic, perhaps because of the "looseness" of the tetramer. Credence in the values recovered for S^2 and τ_e requires a robust (reliable) value for τ_m, perhaps obtained from another technique such as fluorescence anisotropy. However, for reasons we do not understand, the value for τ_m recovered from fluorescence and NMR data for compact (folded) proteins is frequently substantially different, a result that we have noted hitherto (Kemple et al., 1994). Given the inescapable interplay between τ_m and S^2 in the analysis, we believe that this "problem" with τ_m has not been adequately addressed.

(8) There is as yet no good physical or mathematical model to adequately and simply describe peptide backbone motion. This fact makes it difficult to propose the pattern of motion of atoms in the backbone corresponding to the values derived for S^2 and τ_e in peptides. It is clear, however, that peptides are intrinsically less flexible than typical linear organic polymers, and hence, it may not be fully appropriate to use typical polymer theory to describe peptide mobility. Additionally, although the notion of a crankshaft type motion of the peptide bond which derives from molecular dynamics simulations (Daggett et al., 1991) provides a physically attractive model, there has not yet been any attempt to compare experimental values for S^2 and τ_e in particular with the predictions based on such a model.

(9) Finally, the studies of other model peptides of variable length but similar secondary structures, e.g. those developed by Marqusee and Baldwin (1987) or Merutka and Stellwagen (1990), might yield particularly useful information. It is also possible that two-dimensional FTIR methods might provide insights into the nature of conformational exchange between different forms of peptides (B. Pastrana-Rios, D. Graff, S. Venyaminov, and F. G. Prendergast, manuscript in preparation).

ACKNOWLEDGMENT

We thank Dr. Norberto Silva and Mrs. Phyllis Fisher for measurements of $r(t)$, Drs. Slobodan Macura, Nenad Juranic, and Bruce D. Ray for NMR advice and technical assistance at Mayo and the IUPUI NMR Center, respectively, Ms. Madhavilata Adivi for modifications of the computer program used in data analysis, and Ms. Linyang Zhu for order parameter expressions.

REFERENCES

Abragam, A. (1961) *Principles of Nuclear Magnetism*, Chapter VIII, Clarendon Press, Oxford.

Alexandrescu, A., & Shortle, D. (1994) *J. Mol. Biol. 242*, 527−546.

Barbato, G., Ikura, M., Kay, L. E., Pastor, R. W., & Bax, A. (1992) *Biochemistry 31*, 5269−5278.

Bazzo, R., Tappin, M. J., Pastore, J. A., Harvey, T. S., Carver, J. A., & Campbell, I. D. (1988) *Eur. J. Biochem. 172*, 139−146.

Beechem, J. M., & Gratton, E. (1988) *Proc. SPIE-Int. Soc. Opt. Eng. 109*, 70−81.

Blackledge, M. J., Brüchweiler, R., Griesinger, C., Schmidt, J. M., Xu, P., & Ernst, R. R. (1993) *Biochemistry 32*, 10960−10974.

Boyd, J., Hommel, U., & Campbell, I. D. (1990) *Chem. Phys. Lett. 175*, 477−482.

Buck, M., Boyd, J., Redfield, C., MacKenzie, D. A., Jeenes, D. J., Archer, D. B., & Dobson, C. M. (1995) *Biochemistry 34*, 4041−4055.

Buckley, P., Edison, A. S., Kemple, M. D., & Prendergast, F. G. (1993) *J. Biomol. NMR 3*, 639−652.

Chen, C., Feng, Y., Short, J. H., & Wand, A. J. (1993) *Arch. Biochem. Biophys. 306*, 510−514.
Clore, G. M., Szabo, A., Bax, A., Kay, L. E., Driscoll, P. C., & Gronenborn, A. M. (1990) *J. Am. Chem. Soc. 112*, 4989−4991.
Daggett, V., Kollman, P. A., & Kuntz, I. D. (1991) *Biopolymers 31*, 1115−1134.
Dellow, M. J., & Wand, A. J. (1989) *J. Am. Chem. Soc. 111*, 4571−4578.
Dempsey, C. E. (1990) *Biochim. Biophys. Acta 1031*, 143−161.
Fan, F., & Mayo, K. H. (1995) *J. Biol. Chem. 270*, 24693−24701.
Farrow, N. A., Zhang, O., Forman-Kay, J. D., & Kay, L. E. (1995) *Biochemistry 34*, 868−878.
Frank, M. K., Clore, G. M., & Gronenborn, A. M. (1995) *Protein Sci. 4*, 2605−2615.
Friedrichs, M. S., Stouch, T. R., Bruccoleri, R. E., Mueller, L., & Constantine, K. L. (1995) *J. Am. Chem. Soc. 117*, 10855−10864.
Goto, Y., & Hagihara, Y. (1992) *Biochemistry 31*, 732−738.
Hu, Y., MacInnes, J. M., Cherayil, B. J., Fleming, G. R., Freed, K., & Perico, A. (1990) *J. Chem. Phys. 93*, 822−836.
Ikura, T., Gô, N., & Inagaki, F. (1991) *Proteins: Struct., Funct., Genet. 9*, 81−89.
Jarvet, J., Allard, P., Ehrenberg, A., & Gräslund, A. (1996) *J. Magn. Reson. B 111*, 23−30.
Kemple, M. D., Yuan, P., Nollet, K. E., Fuchs, J. A., Silva, N., & Prendergast, F. G. (1994) *Biophys. J. 66*, 2111−2126.
Kinosita, K. S., Kawato, S., & Ikegami, A. (1977) *Biophys. J. 20*, 289−305.
Kuwajima, K. (1989) *Proteins: Struct., Funct., Genet. 6*, 87−103.
Lakowicz, J. R., Maliwal, B. P., Cherek, H., & Balter, A. (1983) *Biochemistry 22*, 1741−1752.
Lefêvre, J.-F., Dayie, K. T., Peng, J. W., & Wagner, G. (1996) *Biochemistry 35*, 2674−2686.
Lipari, G., & Szabo, A. (1982) *J. Am. Chem. Soc. 104*, 4546−4559.
London, R. E., & Avitabile, J. (1978) *J. Am. Chem. Soc. 100*, 7159−7165.
Mackay, J. P., Shaw, G. L., & King, G. F. (1996) *Biochemistry 35*, 4867−4877.
Mandel, A. M., Akke, M., & Palmer, A. G., III (1995) *J. Mol. Biol. 246*, 144−163.
Marqusee, S., & Baldwin, R. L. (1987) *Proc. Natl. Acad. Sci. U.S.A. 84*, 8898−8902.
Mchaourab, H. S., Lietzow, M. A., Hideg, K., & Hubbell, W. L. (1996) *Biochemistry 35*, 7692−7704.
Merutka, G., & Stellwagen, E. (1990) *Biochemistry 29*, 894−898.
Miick, S. M., Casteel, K. M., & Millhauser, G. L. (1993) *Biochemistry 32*, 8014−8021.
Palmer, A. G., III, & Case, D. A. (1992) *J. Am. Chem. Soc. 114*, 9059−9067.
Palmer, A. G., III, Rance, M., & Wright, P. E. (1991) *J. Am. Chem. Soc. 113*, 4371−4380.
Palmer, A. G., III, Hochstrasser, R. A., Millar, D. P., Rance, M., & Wright, P. E. (1993) *J. Am. Chem. Soc. 115*, 6333−6345.
Podo, F., Strom, R., Crifo, C., & Zuauf, M. (1982) *Int. J. Pept. Protein Res. 19*, 514−527.
Small, E. W., Libertini, L. J., Brown, D. W., & Small, J. R. (1991) *Opt. Eng. 30*, 345−356.
Terwilliger, T. C., & Eisenberg, D. (1982a) *J. Biol. Chem. 257*, 6010−6015.
Terwilliger, T. C., & Eisenberg, D. (1982b) *J. Biol. Chem. 257*, 6016−6022.
Valeur, B., & Weber, G. (1977) *Photochem. Photobiol. 25*, 441−444.
Weaver, A. J., Kemple, M. D., & Prendergast, F. G. (1989) *Biochemistry 28*, 8624−8639.
Wishart, D. S., Sykes, B. D., & Richards, F. M. (1991) *J. Mol. Biol. 222*, 311−333.
Wishart, D. S., Bigam, C. G., Yao, J., Abildgaard, F., Dyson, H. J., Oldfield, E., Markley, J. L., & Sykes, B. D. (1995) *J. Biomol. NMR 6*, 135−140.
Yuan, P., Fisher, P. J., Prendergast, F. G., & Kemple, M. D. (1996) *Biophys. J. 70*, 2223−2238.
Zhu, L., Kemple, M. D., Landy, S. B., & Buckley, P. (1995a) *J. Magn. Reson. B 109*, 19−30.
Zhu, L., Kemple, M. D., Yuan, P., & Prendergast, F. G. (1995b) *Biochemistry 34*, 13196−13202.

BI962146+